Chapter 10
Instruments for Observations of Radioactivities

Gottfried Kanbach and Larry Nittler

This chapter describes key tools used to observe cosmic radioactivity including astronomical methods, laboratory measurements of meteorites and detection of Galactic cosmic rays. Cosmic nucleosynthesis, that is, the creation of new elements including radioactive isotopes, occurs in the most energetic, often explosive, sites in the universe. To observe these targets and processes in the light of high-energy photons, which are emitted in nuclear transitions and particle interactions, sensors for photon energies from around 100 keV to more than 10 MeV have been developed and employed on satellites and balloon platforms, outside the Earth's atmosphere, which is opaque to this radiation. The basic interactions for such photons are the photoelectric effect, Compton scattering, and pair creation. Typical examples for instrument designs are described in the first section of this chapter, followed by a presentation of successful missions since the 1980s (SMM, Compton Gamma-Ray Observatory CGRO), then currently operational missions (INTEGRAL, NuStar, Fermi), and perspectives for future telescopes with advances in technology. The second section addresses radioactivities in meteorite samples, which are generally measured by means of mass spectrometry. The most widely used methods are thermal ionisation (TIMS), multi-collector inductively-coupled-plasma (MC-ICPMS), secondary ion- (SIMS), and resonance ionisation mass spectrometry (RIMS). Parent and daughter nuclides can be measured on a variety of sample sizes, with precision depending on the size of the sample and concentrations of the elements of interest. The ultimate attainable precision is generally limited by the number of atoms in a given sample. New developments

G. Kanbach
Max Planck Institut für extraterrestrische Physik, Garching, Germany
e-mail: gok@mpe.mpg.de

L. Nittler (✉)
Carnegie Institution for Science, Washington, DC, USA
e-mail: lnittler@ciw.edu

R. Diehl et al. (eds.), *Astrophysics with Radioactive Isotopes*, Astrophysics and Space Science Library 453, https://doi.org/10.1007/978-3-319-91929-4_10

in RIMS, accelerator-based SIMS, and laser-assisted atom-probe tomography all hold promise for pushing meteoritic measurements to higher sensitivity and smaller spatial scales. Galactic cosmic rays are addressed in a third section. These are analysed by a variety of instruments from the ground, on high altitude balloons, or on spacecraft. Basic principles are discussed as well as specific experiments, including the Pierre Auger Observatory, the Cosmic Ray Isotope Spectrometer on the ACE spacecraft, TIGER, and PAMELA.

10.1 Astronomical Telescopes

10.1.1 Measuring Radiation from Cosmic Radioactivity

10.1.1.1 General Considerations

Radioactivity is characterised by the emission of particles or photons that accompany the nuclear transformations of unstable isotopes. Direct observations of secondary particles (e.g., $\beta^{\pm}$, or α) are only possible with in-situ measurements in the *local environment* of the solar system and often the detected particles are not very specific as to their parent nuclei. Transitions between energy levels of radioactive and excited nuclei however produce characteristic X- and γ-ray lines that can be detected from astronomical distances. Only one secondary *particle* resulting from radioactive decay, the positron, signals its presence in a characteristic γ-ray line: positrons annihilate with their anti-particle (electrons) and convert the pair's rest mass into a line at 511 keV (see Chap. 7). Nuclear energy levels range from the atomic levels at 10s of keV upwards to energies of 10s of MeV with most important astrophysical lines in the range from about 100 keV to several MeV.

Detection of MeV photons must exploit the dominant interaction processes in this energy range: the photoelectric effect (*'photoeffect'*) and *Compton scattering*. Both these interaction processes and their cross-sections depend on photon energy and target material. The typical energy of transition from dominating photoeffect to Compton scattering is around the rest mass energy of the electron, i.e. 511 keV. For photon energies above the highest atomic binding energy the photoelectric cross section is given by $\sigma \propto Z^n E^{-3}$, where Z is the atomic number (of protons) and n is an index with a value between 4 and 5. At lower photon energies characteristic line-structures appear in the cross section (K-, L-, M-edges, etc.) which indicate the atomic energy levels of the electrons released in an atomic transition. The experimental consequence is that a high-efficiency photoelectric detector should be made of high-Z material, and it will work best below a few 100 keV. Spectroscopy with such detectors however requires careful calibration, because these structures in the cross section will shape the instrumental response and appear in the measurements. At higher energies, incoherent scattering of photons with electrons, (*Thomson* and *Compton scattering*), leads to the release of an energetic electron and a secondary photon, and dominates photon interactions. The

maximum of this interaction cross section is around 511 keV ($m_e c^2$). The high- and low-energy ends of the cross section behavior can be described by asymptotic limits in terms of the *Thomson* cross section

$$\sigma_T = \frac{8\pi}{3}\left(\frac{\alpha\hbar}{m_e c}\right)^2 \simeq 6.652 \times 10^{-25}\,\mathrm{cm}^2 \tag{10.1}$$

and the photon energy in units of the electron rest mass, $\epsilon = h\nu/m_e c^2$. In the *Thomson regime*, $\epsilon \ll 1$, the total cross section is about $\sigma = \sigma_T(1 - 2\epsilon \ldots)$. In the high energy limit (the *Klein Nishina* regime, $\epsilon \gg 1$) the total cross section is a decreasing function of energy:

$$\sigma = \frac{3}{8}\sigma_T \epsilon^{-1}(1 + 2\ln\epsilon) \tag{10.2}$$

Detailed tables of photon cross sections for various elements and compounds are available at http://physics.nist.gov/PhysRefData/Xcom/Text/XCOM.html.

10.1.1.2 Instrument Types

Building an efficient detector for ~MeV gamma radiation however not only demands a good choice of detector material, but also requires that the detectors are sensitive to measure the secondary particles (electrons, positrons) released by the incoming energetic photons. This can be achieved in several ways:

- **Ionisation chambers:** the detector is intrinsically capable of measuring the presence of ionisation and generating an electronic signal. Gas-filled ionisation chambers, proportional counters, or Geiger counters were the original devices to detect high energy radiation. The small amounts of charge generated in the detector volume by a single photon is often amplified by a strong electric field generated from electrodes. This results in acceleration, collisional secondary ionisation and the formation of a break-down cascade, that is more easily detectable. Variations of this principle led to gas-filled drift chambers or spark chambers that also allowed to locate the impact coordinates of primary photons. After semiconductors with sufficient volume had been developed (e.g. Si, Ge, Cadmium Zinc Telluride, CZT, or Cadmium Telluride, CdTe) the principles and concepts of ionisation chambers were transferred to the new solid state detectors. The higher densities and generally higher atomic numbers of solid state detectors led to much higher efficiencies for the conversion of γ-rays and, in the case of cryogenically cooled detectors, also to very fine energy resolution (Ge detectors).
- **Scintillation detectors:** the detector material emits light under the impact of ionisation (*fluorescence, scintillation*). In addition to the scintillator material itself, these detectors require a photon detector to record the emitted light. Commonly used are *organic scintillators* (liquid or solid), scintillating *crystals*

(e.g., NaI, CsI, BGO, La_2Br_3), or *noble gases* (e.g., liquid Xenon). Traditionally the detection of scintillation light was achieved with *photo-multiplier tubes (PMTs)*, which are low noise and very fast detectors. The typical quantum efficiency of a PMT photocathodes however is only around ∼20%. More recently the readout of scintillation light is also done with *solid-state photodetectors* such as PIN diodes, Si drift detectors (SDD), and avalanche photo diodes (APD). The advantages of solid state readout are a higher detection efficiency, the small size and the possibility of complex arrangements (pixels, arrays) of Si detectors, in addition to the straightforward interface with modern readout electronics.

All high energy detectors in space are exposed to radiation of energetic particles (cosmic rays, radiation belts) and thus *photons of non-astronomical origin*. The structures of spacecraft and detector alike will become sources of local background under this irradiation. Direct nuclear interactions and the creation of radioactive isotopes may lead to intense levels of background, unless counter measures are taken. Direct and prompt interactions of incident charged particles can be rejected by enclosing the sensitive volumes in veto shield detectors. These *anti-coincidence* detectors are often made of plastic scintillator (e.g., *COMPTEL*, Schönfelder et al. (1993), *EGRET*, Kanbach et al. (1989), *Fermi*, Atwood et al. (2009)) but massive shields of inorganic scintillators, like *CsI (SMM-GRS*, Forrest et al. (1980)) or *BGO (INTEGRAL-SPI*, Vedrenne et al. (2003)) are also employed to better cover the low energy range. There is a trade-off to be made between adding detection capability for undesired events and adding mass which generates such undesired events.

To improve handling of the *intrinsic background* of a gamma-ray telescope, several options are available:

- The structural materials close to the sensitive detectors should be chosen specifically to ensure low activation by the dominant external particle environment (i.e., low cross sections for such reactions). For example, aluminium, which activates to radioactive ^{24}Al, could be replaced by beryllium; hydrazine propellant, which thermalises and captures neutron on protons, emitting 2.2 MeV photons, should be minimised.
- The sensitive parts of a detector could be mounted at a distance from the mass of the spacecraft, e.g., on a boom.
- the detection process should fully exploit the characteristics of gamma-ray interactions to discriminate against background through selections in the measured interaction details. Examples that have been used include *pulse shape discrimination* to separate neutron and γ-ray interactions or specific coincidence trigger requirements.
- The *choice of orbit* of a low-energy gamma-ray telescope should avoid regions of elevated particle background in the Earth's magnetosphere (radiation belts, South Atlantic Anomaly). A low altitude, circular equatorial orbit provides the best environment for such telescopes, since it is also shielded against low energy solar particles.

Even with the above counter measures, the instrumental background of a nuclear line telescope will remain at a significant level and often dominates celestial signals even for strong sources (see Chap. 7). The spectrum of this background extends from several 100 keV up to about 5 MeV and shows a continuum and several strong complexes of nuclear lines. Detailed simulations are essential, and were developed based on the Monte-Carlo principle and detailed high-energy interaction physics software packages such as *GEANT*, e.g., by Weidenspointner et al. (2005). This allows one to estimate the intensity and spectrum of instrumental background, for future and past missions. Simulations and trade-offs for options of telescope design and orbit can thus be investigated.

The usefulness of an astronomical telescope can be expressed as the level of *sensitivity* reachable during typical periods of observation. Sensitivity is given as the minimum source flux that can be detected significantly above the level of background. Generally the instrumental-background signature is spread out, and varies smoothly over the field of view, but it contains the spectral features mentioned above. In a telescope with temporal, angular and energy resolution, the relevant level of background is then the level contained in the temporal, angular and spectral resolution elements which would be populated by the signal from a real source (*point spread function*). The resolution elements of measurement and analysis, i.e., bins in a measured signal parameter, pixels in an image, or $\Delta E/E$ in a spectrum, should therefore correspond to the properties of the astronomical sources in order to optimize the sensitivity. Of course the combination of angular and spectral resolution will lead to best results, but as we discuss below, temporal resolution for transient or variable sources (flares, bursts) may well substitute a lack of angular resolution. We discuss now typical examples of successful instruments, that pioneered nuclear-line astrophysics.

10.1.2 Photon Collectors

SMM-GRS, the γ-ray spectrometer of the *Solar Maximum Mission (SMM)* was an actively shielded multi-crystal scintillation γ-ray spectrometer with a wide field of view, sensitive to γ-rays in the energy range from about 300 keV to 100 MeV (Forrest et al. 1980). Its goal was to measure solar flares and during the mission from 1980 to 1989 a total of 185 flares were detected (Vestrand et al. 1999). The discrimination of signal and background in *SMM-GRS* was based on the time profile of the flares riding on top of a slowly varying background and on a model of the orbital background averaged over locations of similar magnetospheric conditions. *SMM-GRS* was therefore a typical photon collector with little angular resolution. The γ-ray spectrometer, shown in Fig. 10.1, was composed of 7 cylindrical NaI(Tl) crystals with a diameter of 7.6 cm and a height of 7.6 cm. Each of these crystals was viewed by a PMT. The crystals were surrounded on the sides by a 2.5 cm thick CsI annulus. On the rear side a circular CsI crystal with a thickness of 7.6 cm and a diameter of 25 cm was placed. The 7 NaI (Tl) crystals and the back CsI crystal

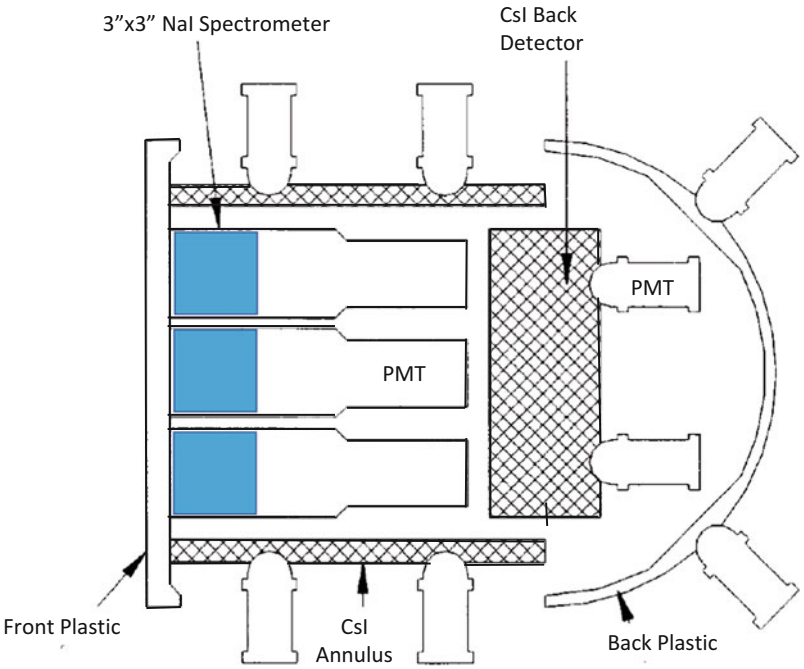

Fig. 10.1 The *Gamma Ray Spectrometer* on the *Solar Maximum Mission* (Forrest et al. 1980). Seven 3" NaI detectors are enclosed in an anti-coincidence shield made of a plastic scintillator (front and back) and of CsI scintillators (sides and back)

formed together the high-energy detector. In order to suppress charged particles the front and rear sides were covered with sheets of plastic scintillators thus shielding the main detector from all sides. The γ-ray spectrometer had a very wide field of view with a diameter of $\simeq 120°$, an energy resolution of 7% at 662 keV and an effective area ranging from 20 to 200 cm^2 as a function of energy.

10.1.3 Imaging Instruments

COMPTEL was the first truly imaging telescope for the MeV range and was in orbit for 9 years from 1991 to 2000 (Schönfelder et al. 1993) aboard NASA's *Compton Gamma-Ray Observatory*. A photomontage of *COMPTEL* is shown in Fig. 10.2.

The upper detector, called D1, consists of 7 modules filled with the liquid scintillator NE 213A. Each module of 28 cm diameter and 8.5 cm thickness is viewed from the sides by 8 photomultiplier tubes. The total geometrical area of D1 is 4300 cm^2. The lower detector, D2, separated from D1 by 1.5 m, consists of 14 modules of NaI(Tl)-scintillator. Each module of 28 cm diameter and 7.5 cm thickness is viewed from below by 7 photomultipliers. The total geometrical area

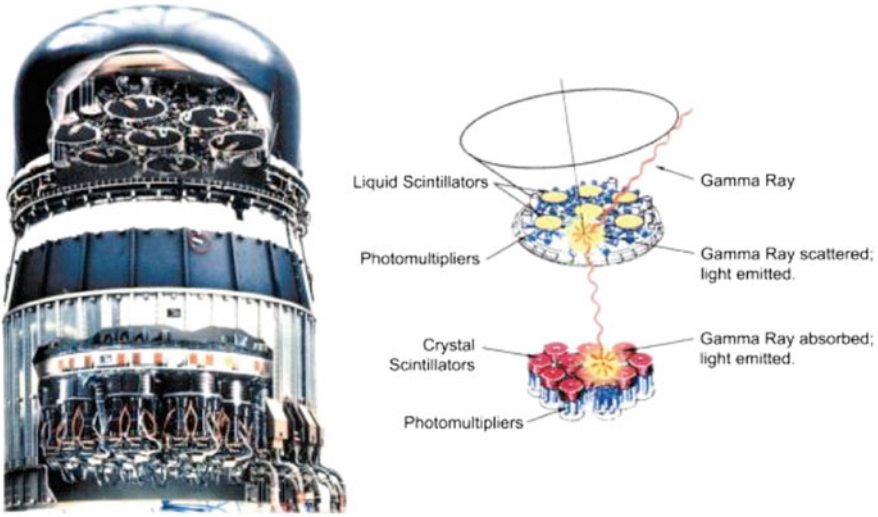

Fig. 10.2 The *COMPTEL* instrument on the *Compton Gamma Ray Observatory CGRO* (Schönfelder et al. 1993). A schematic drawing shows a typical scattering event and the cone with opening angle ϕ which contains the incident photon

of D2 is 8600 cm^2. From the relative pulse heights of the photomultiplier tubes in each D1- and D2-module the locations of the interactions are determined to within about 2 cm. The sum of the photomultiplier signals of each module provides the energy losses E1 and E2 . Both, D1 and D2 are completely surrounded by veto-domes of 1.5 cm thick plastic scintillator to reject charged particles. A valid event trigger is generated by a time-of-flight delayed coincidence between D1 and D2 and the absence of a veto signal. The positions of the interactions in D1 and D2 define the direction of the scattered photon and the Compton scattering formula

$$cos(\phi) = 1 - m_e c^2 (\frac{1}{E2} - \frac{1}{E1 + E2})$$

is used to estimate the opening angle of a cone that contains the incident gamma ray (see schematic in Fig. 10.2)

COMPTEL covers the energy range 0.8–30 MeV. Within its large field-of view of about 1 steradian (64°, FWHM), its angular resolution rages from 1.7° to 4.4° (FWHM; depending on energy). The energy resolution is in the range 5–8% (FWHM), and the effective detection area is in the range 20–30 cm^2 (again depending on energy). The sensitivity of *COMPTEL* is significantly determined by the instrumental background. A substantial suppression is achieved by the combination of the charged particle veto domes, the time-of-flight measurement technique, pulse shape discrimination in D1, Earth horizon angle cuts, and proper event selection cuts. In spite of these significant countermeasures the actual total

in-flight instrumental background was higher than expected prior to launch by about a factor of 4. As a consequence, the sensitivity of *COMPTEL* was a factor of two worse than expected. Fortunately, however, this loss in sensitivity could be compensated by the four times longer mission life-time (which originally was planned to be only 2.25 years). The actually achieved point source sensitivity for deep observations ($T = 6 \times 10^6$ s) was 6.3×10^{-5} photons/cm^2 s for continuum emission between 1 and 30 MeV (corresponding to about 3% of the Crab-flux) and 1.6×10^{-5} photons/cm^2 s for line emission at 1.157 and 1.809 MeV (^{44}Ti and ^{26}Al lines).

10.1.4 Current Spectrometry and Imaging: INTEGRAL/SPI, NuSTAR, and COSI

As we have discussed above, angular resolution is an essential requirement to achieve astronomical sensitivity. When the spectrometer instrument for ESA's INTEGRAL mission was designed it was clear that the superb energy resolution of a Ge spectrometer had to be combined with a telescope that provides at least moderate angular resolution. In the Spectrometer for Integral, SPI, this was achieved with a coded-mask system (see Fig. 10.3). The SPI mask, which is mounted 171 cm above the detection plane, features a HURA (for 'Hexagonal Uniform Redundant Array') coded mask pattern with 120° symmetry enclosed within a diameter of 72 cm. Of the 127 individual cells (60 mm side to side) in the mask, 63 are opaque (3 cm thick blocks of Densimet, a tungsten alloy, with an opacity of about 90%) and 64 are transparent. The *shadowgram* projected onto the detector plane is measured with 19 Ge detectors. The reverse-electrode n-type Ge detectors also have a hexagonal shape with a side length of 3.2 cm and a height of 69.42 mm and are operated at a temperature of ~90 K cooled by a Sterling system. The detector is enclosed in a massive anti-coincidence shield of BGO scintillation detectors. The energy range extends from 20 keV to 8 MeV with a typical energy resolution of 2.5 keV at 1.33 MeV. The coded mask system provides an angular resolution of about 2.5° with a positioning accuracy for a strong source of 10 arc min. The fully coded field-of-view has a diameter of 16°. Further details can be found in Vedrenne et al. (2003). ESA's INTEGRAL observatory with its main instruments SPI (spectrometer) and IBIS (imager) was launched on October 17, 2002 and has been operating successfully since then (Diehl et al. 2017). Several astrophysical results from INTEGRAL/SPI observations address radioactivities and are described in Chaps. 4–7 of this book.

The NASA small explorer mission *NuSTAR* (Nuclear Spectroscopic Telescope Array) was launched on June 13, 2012. NuSTAR employs two co-aligned grazing incidence X-ray telescopes with a focal length of about 10 m. These nested Wolter-1 type optics are coated with multilayers allowing effective reflection of X-rays in the energy range 3–79 keV. Each of the two focal plane detectors consists of a 2 × 2

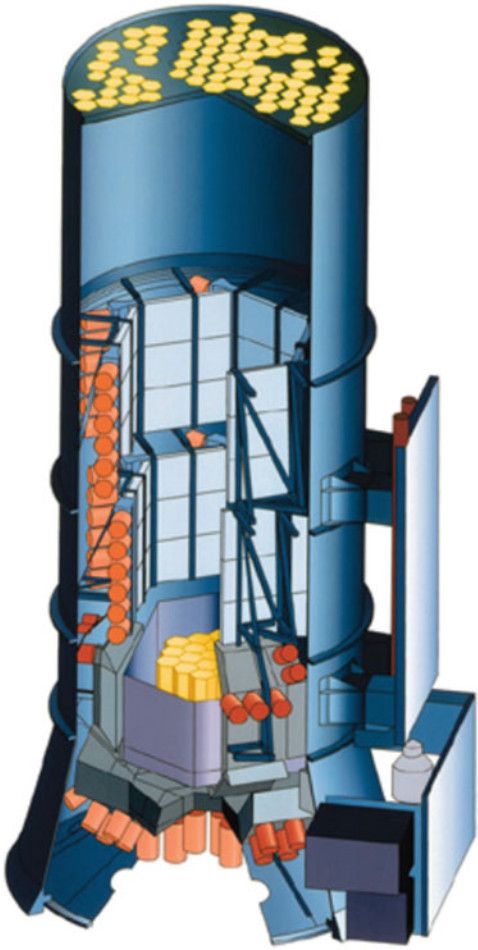

Fig. 10.3 The *Spectrometer Instrument (SPI)* on ESA's *INTEGRAL* mission (Vedrenne et al. 2003). The γ-ray sky is projected through a coded mask onto an array of 19 Ge detectors. Deconvolution of the shadowgram allows an angular resolution of 2.5 deg and the Ge detectors provide an energy resolution $E/\Delta E$ of ~600

array of CdZnTe pixel detectors, each with 32 by 32 pixels, 0.6 mm in size. With a field of view between 10 arcmin (at 10 keV) and 6 arcmin (at 68 keV), NuSTAR achieves an angular resolution of 18 arcsec (FWHM). The prime objectives of this telescope are therefore the observation of galactic and extra-galactic point sources and small scale structures such as young SNe. The effective area of NuSTAR in the range around 70 keV, which is relevant for some low energy radioactivity, is about 60 cm^2. A full description of NuSTAR is given by Harrison et al. (2013). A major result from NuSTAR was the imaging of radioactive debris in the supernova remnant Cas A, where the ^{44}Ti decay lines at 68 and 78 keV were used for locating the radioactive ^{44}Ti and determining its kinematics (see Chap. 4).

The balloon experiment *COSI* (Compton Spectrometer and Imager) is based on Ge detector units that record Compton interactions in the photon energy range 0.2–5 MeV. The compact Compton telescope design consists of 12 cross-strip,

high-purity germanium detectors, each of size $8 \times 8 \times 1.5\,\mathrm{cm}^3$ with strip read-out electronics allowing 3-dimensional resolution. The total active detector volume is $972\,\mathrm{cm}^3$. In May 2016 the COSI instrument was flown for 46 days on NASA's new super pressure balloon; launched from Wanaka, New Zealand the balloon circled around the globe one and a half times and landed in Peru. The instrument and preliminary results from this balloon campaign are described in Kierans et al. (2017).

10.1.5 Perspectives of Cosmic Gamma-Ray Imaging and Spectroscopy

In the years since the termination of the *CGRO* mission, many efforts and studies were undertaken to develop the next generation of Compton telescopes. Some projects, such as the *Advanced Compton Telescope ACT* (Boggs et al. 2006), *GRIPS* (Greiner et al. 2009), and *GRI* (Knödlseder 2007) were proposed to the space agencies but were not selected. Other experiments were built as prototypes or balloon payloads. Among those are MEGA (Kanbach et al. 2003), the *Nuclear Compton Telescope NCT* (NCT Collaboration et al. 2007), and *TIGRE* (Zych et al. 2006).

A very compact instrument using a Compton scattering technique—the Soft Gamma Ray Detector, *SGD*, was developed for the Japanese mission *ASTRO-H* (Takahashi et al. 2009, 2004). The Compton camera *SGD* was built with Si and CdTe detectors and was surrounded by an active BGO shield. Its energy range was 40–600 keV. After launch on Feb. 17, 2016, the mission was named *HITOMI*. Unfortunately the satellite was lost due to a malfunction of the attitude control system on March 26, 2016 and only very few useful observations were recovered.

Two gamma-ray telescopes covering the range from about 300 keV up to 10s of GeV are currently (2017) being studied in the U.S. (*AMEGO*) and in Europe (*e-ASTROGAM*). Both concepts combine the capabilities of the major *CGRO* instruments: *COMPTEL* in the Compton range from 300 keV to about 10 MeV and *EGRET* in the pair creation range (>10 MeV) in a large instrument that records both types of interactions. These telescopes are based on modern solid-state detectors and feature large fields of view (>2 sr), angular resolution of $\sim$1–3 deg, and energy resolution of $\sim$10 keV in the range of nuclear lines. Polarisation sensitivity is a further goal of high interest in gamma-ray astronomy.

The European *e-ASTROGAM* mission (De Angelis et al. 2017) features a deep tracker unit made of Si strip detectors that allows imaging of the secondary particles released in Compton scattering or pair creation events. The total energy of the incoming photons is partially measured in the tracker and finally deposited in a massive calorimeter made of CsI scintillators. The gamma-ray telescope is surrounded by an anticoincidence veto shield of plastic scintillator to reject charged background radiation. In Fig. 10.4 the expected sensitivity of the e-ASTROGAM

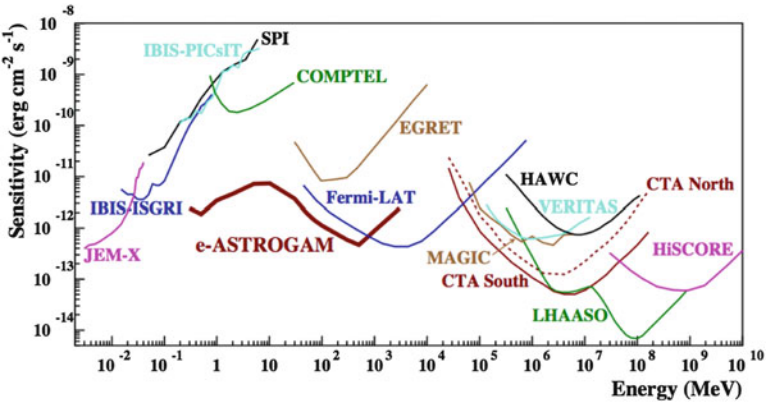

Fig. 10.4 Point source continuum sensitivity of different X- and gamma-ray instruments. The curves for INTEGRAL/JEM-X, IBIS (ISGRI and PICsIT), and SPI are for an observing time Tobs = 1 Ms. The COMPTEL and EGRET sensitivities are given for the time accumulated during the duration of the CGRO mission (about 9 years). The Fermi/LAT sensitivity is for a high Galactic latitude source over 10 years. For MAGIC, VERITAS, and CTA, the sensitivities are given for $T_{obs} = 50$ h. For HAWC $T_{obs} = 5$ years, for LHAASO $T_{obs} = 1$ year, and for HiSCORE $T_{obs} = 1000$ h. The e-ASTROGAM sensitivity is for an effective exposure of 1 year for a source at high Galactic latitude (adapted from De Angelis et al. 2017)

gamma-ray telescope is shown. The range of nuclear lines between ~300 keV up to ~10 MeV is well covered by *e-ASTROGAM* with a sensitivity that exceeds previous coverage by more than an order of magnitude.

The mission *AMEGO* (All-sky Medium Energy Gamma-ray Observatory, McEnery 2017) is under study by a large collaboration in the U.S. The basic design is similar to *e-ASTROGAM*, and the use of pixelated CdTe detectors in the calorimeter enhances the low energy response of *AMEGO* between 200 and 300 keV.

From *COMPTEL* and *INTEGRAL*, we have learned that the sky is rich in phenomena and objects that can be studied around 1 MeV. But it is also true, that with *COMPTEL* we could see only the tip of the iceberg. The achieved sensitivity was still modest. The next telescope will have to have sensitivity better than an order of magnitude. In the studies listed above different concepts of Compton telescopes are presently investigated and tested. Instead of scintillators also other detector materials are considered and tested, like silicon strip detectors, position sensitive germanium detectors, CdTe-detectors, liquid xenon gas detectors, and high pressure gas detectors. In order to achieve the required improvement in sensitivity, the detection efficiency has to be drastically increased and the background has to be reduced considerably. Several of the proposed experiments are capable of achieving this higher level of sensitivity and hopefully will advance gamma-ray astronomy in this largely undeveloped MeV wavelength band. What is needed is a decision by the international space agencies that this window into the universe is worth exploring

with a new mission with a sensitivity to go beyond the *tip of the iceberg* results addressed in Chaps. 4–7.

10.2 Analyzing Material Samples from and Within Meteorites

Radioactivities in meteorite samples are in general detected by separating individual atoms from a sample and weighing them with a device known as a mass spectrometer. For long-lived radionuclides, that is those with lifetimes significantly longer than the 4.6 billion year age of the Solar System, the nuclides themselves are detected, along with their decay products. In the case of short-lived isotopes created by cosmic-ray interactions with the meteorites during the time interval between ejection from a parent body and arrival on Earth, the parent isotopes can also be directly measured. For short-lived isotopes that existed in the early Solar System but have since fully decayed (*extinct* isotopes), only the decay products can now be determined. In most cases, stable isotopes of the parent and daughter elements must also be measured in order to derive reliable information. Depending on the sample and the isotopic system, a wide array of instrumentation and techniques can be used to derive information on radioactive elements in extraterrestrial samples. These are the subject of this section.

10.2.1 Measurement Principles and Techniques

When a radionuclide decays within a solid sample, the isotopic compositions of both the parent and daughter elements are changed. By plotting isotopic and/or elemental ratios, one can infer either the age of the sample (time elapsed since the sample solidified to the point that the parent isotope was fixed in the structure) or, for extinct isotopes, the initial abundance of the parent isotope. This is illustrated in Fig. 10.5, which shows an example of *Rb-Sr* dating based on the decay of long-lived ($\tau \sim 7.2 \times 10^{11}$ years) ^{87}Rb to ^{87}Sr. Each plotted point represents a different mineral that obtained a different Rb/Sr elemental ratio upon crystallisation of the rock. Initially all of the minerals had the same ^{87}Sr/^{86}Sr ratio (open circles), but with time, some of the ^{87}Rb decayed, moving the points to the up and left on the plot (filled symbols). The age of the rock can be calculated from the slope of the resulting line; this line is called an *isochron.*

For the case of extinct nuclides, the daughter isotope ratio is plotted versus a stable isotope of the parent element, and the slope of an isochron gives the initial ratio of the extinct nuclide to the stable isotope. For example, to detect extinct ^{26}Al, one plots the measured ^{26}Mg/^{24}Mg ratio versus the ^{27}Al/^{24}Mg ratio and the slope gives the initial ^{26}Al/^{27}Al ratio of the sample (see Chap. 6). Often, one seeks information on a single object with a single parent/daughter element ratio, for example pre-solar grains (Chap. 3). In such cases, isochrons cannot be constructed

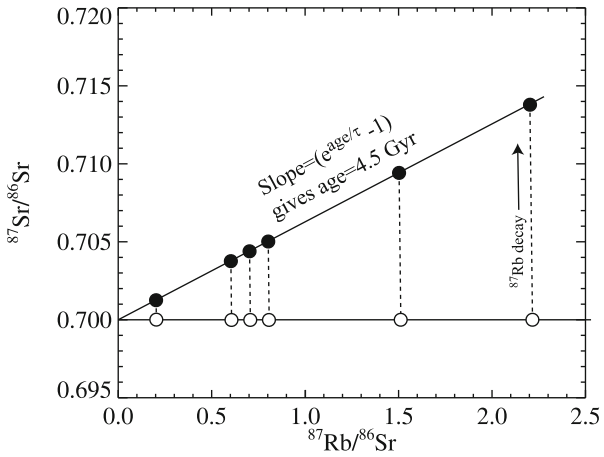

Fig. 10.5 Schematic example of radiometric dating of rocks. Open symbols represent the initial isotopic compositions of a set of minerals that co-formed with varying Rb/Sr ratios. After 4.5 Gyr, some of the long-lived ^{87}Rb has decayed to ^{87}Sr (filled symbols); the slope of the resulting *isochron* gives the age of the rock

and assumptions regarding the initial stable isotopic composition must be made to determine initial abundances of radionuclides. Usually, such assumptions can be made with sufficient confidence for the problem at hand.

Note that there are many complications to radiometric age-dating and determination of extinct isotopes, both arising from the laboratory analyses (see below) and from the samples themselves. For example laboratory contamination can compromise analyses, especially for very-low-abundance elements. Atoms of either the parent and/or daughter elements may have diffused over time into or out of the sample, so that the measured ratios do not reflect the simple isochron behaviour described above. Researchers have developed many techniques for identifying and overcoming such problems.

Mass spectrometers determine the elemental, isotopic or molecular composition of a sample by first converting the atoms or molecules of the sample into a beam of ions and then using electric and/or magnetic fields to disperse the beam in mass. Thus every mass spectrometer requires an ion source, a filter to separate masses and one or more ion detectors. Several examples of different types of mass spectrometers used for meteoritic radioactivity research are detailed in subsequent sections. However, we note here that a key distinction must be made between *bulk* analyses—those that are made on relatively large samples, usually chemically treated to concentrate the elements of interest, and *in situ* analyses—those that sample specific locations within a solid sample. For bulk analyses, the sample may be a single mineral grain a few hundred microns in size up to several grams of a whole meteorite. The sample is first dissolved in pure acids and other solvents and then chemical techniques (e.g., cation exchange columns) are used to purify the element(s) of interest. For *in situ* measurements, no chemical preparation

is necessary; polished rock sections or dispersed mineral grains can be directly sampled by the instrumentation, down to sub-micron spatial scales.

Which technique is used for a specific problem depends on the problem itself, but is largely a question of sample size, abundances of the elements of interest and the required analytical precision. Because fundamentally this work involves counting atoms, the ultimate precision depends on the number of atoms that can be measured in a given sample. Since the magnitude of a radiogenic isotope effect depends on the parent/daughter ratio (e.g., Fig. 10.5), the lower this ratio is, the higher a precision is required and thus the larger number of atoms must be counted. In general, the highest precisions can be obtained with bulk techniques, but the attainable precision of modern *in situ* instrumentation has greatly increased in recent years, any many problems can now be addressed at smaller scales than was historically possible.

Most of the mass spectrometers described below use a magnetic-sector design for mass filtering the ion beam, often with an additional electrostatic analyser (ESA) for double-focusing the beam in energy and mass. For example, Fig. 10.6 shows a schematic diagram of the NanoSIMS 50L ion microprobe (Cameca Instruments)

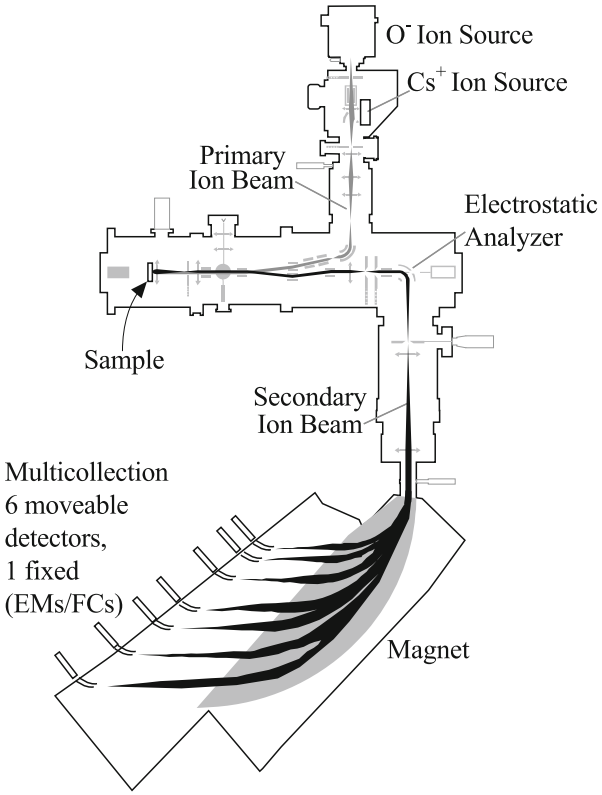

Fig. 10.6 Schematic illustration of Cameca Instruments NanoSIMS 50L ion microprobe

used for many *in situ* measurements of pre-solar grains and other meteoritic components. In this double-focusing mass spectrometer, the ESA is used to disperse the beam of ions from the sample according to kinetic energy and an electromagnet is used to disperse the beam in mass/charge ratio. The ESA and magnet are matched such that ions of a given mass/charge ratio are brought to the same focal point regardless of their kinetic energy.

The most common detectors used for meteoritic mass spectrometry are Faraday Cups (FCs) and electron multipliers (EMs). FCs measure the total charge deposited in a small conductive cup; they have essentially 100% detection efficiency but electronic noise requires minimum ion currents of $>10^4$ $-10^5\,s^{-1}$ for accurate measurements. In an EM, a single ion triggers an exponentially increasing cavalcade of electrons, which generates a measurable electronic pulse. EMs are thus used for low-counting-rate situations. However, in general the detection efficiency of an EM is less than unity, varies with element (and isotope) and changes with time as it is bombarded with more and more ions (*aging*). These problems limit the ultimate precision that may be attained by measurements that use EMs, compared to those that use FCs. Some mass spectrometers are built with a single ion detector. In these systems, the current in the magnet is repeatedly changed (*peak-jumping*) in order to focus different isotopes onto the detector. Repeated cycles of peak-jumping are used to build up statistics for the isotopes of interest and calculate ratios. In contrast, in a *multi-collection* system (e.g., Fig. 10.6), the magnet spreads the ion beam out along its focal plane so that different isotopes are measured simultaneously in a set of detectors. Multi-collection both decreases the time required for analyses and improves the accuracy of measurements compared to peak-jumping.

Other types of mass spectrometry, including accelerator mass spectrometry (AMS), gas-source mass spectrometry, and several types of organic mass spectrometry, while used for some meteorite research, are not used commonly for research related to the topics of this book and are not discussed further here. The exception is AMS, used for nuclear reaction rates, and described in Chap. 9, and for analysis of material samples of solar-system probes that hold traces of cosmic radioactivity (see Fig. 10.7; discussed in Chaps. 4 and 7).

10.2.2 Bulk Techniques

The most commonly-used methods for bulk isotopic analysis of meteoritic components are Thermal Ionisation Mass Spectrometry (TIMS) and Multi-Collector Inductively-Coupled Mass Spectrometry (MC-ICPMS). In TIMS, the element to be analysed is chemically separated from the sample, and deposited from aqueous solution onto a metal (commonly W, Re, or Ta) filament. As the filament is heated by an electric current, atoms from the sample boil off and become ionised. The ions then pass through a magnetic mass spectrometer and are counted, usually by a multi-collection system of Faraday Cups. TIMS has the advantages of very high transmission of ions to the detectors as well as producing very stable beams,

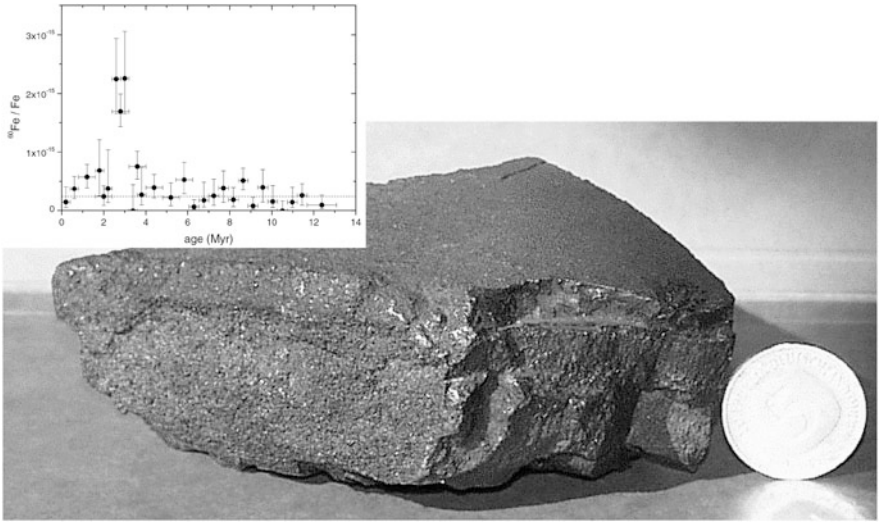

Fig. 10.7 A sample of ocean crust from the deep Pacific ocean. Such a crust grows slowly but steadily from material sedating at a few mm per 1000 years. The fraction of radioactive ^{60}Fe nuclei was enough so that with sensitive accelerator mass spectrometry its detection was possible, and lead to the enrichment history diagram shown in the inset, using depth dating with radioactivity of ^{10}Be and ^{53}Mn (Knie et al. 2004)

especially for elements with relatively low ionisation potentials, such as Mg, Cr, Fe, Ni, Sr, Pb and many others. For example, the original discovery of extinct ^{26}Al in the Solar System was made by TIMS measurement of Mg isotopes (Gray 1974; Lee et al. 1976). However, the thermal ionisation processes introduces a mass fractionation, such that lighter atoms more easily get ionised, and the data must be corrected for this. Quantification of concentration ratios of different elements (needed to determine radiometric ages and abundances of extinct isotopes, see above) is accomplished by isotope dilution, where a known amount of artificially-enriched isotopic tracers are added to the sample and measured along with the isotopes of interest.

In bulk MC-ICPMS analysis, drops of a solution of purified element are sprayed into an Ar plasma at very high temperature. The plasma evaporates the droplets and ionises the sample atoms with high efficiency and the ions are then passed through a multi-collector double-focusing mass spectrometer. MC-ICPMS has the advantages of high ionisation efficiency for all elements, including some elements difficult to measure by TIMS (Lee and Halliday 1995), as well as relatively rapid data collection. As in TIMS, mass fractionation effects are significant and must be corrected for, often by measuring standards with known isotopic composition.

10.2.3 In Situ Techniques

In addition to being used for bulk analyses, MC-ICPMS instruments can be equipped with a laser system for *situ* analysis. A UV laser (e.g., 193 nm) is focused into a ~10–100 μm spot on a sample, ablating material that is then transferred into the Ar plasma. High precisions can be obtained, but this method has the disadvantage that all elements in the sample are transferred to the plasma and ionised, leading to the possibility of unresolved isobaric interferences in mass spectra. Nonetheless, the technique has been successfully applied to studies of extinct radioactivity in meteorites (Young et al. 2005).

The most widely used *in situ* mass spectrometric technique for meteoritic research is Secondary Ion Mass Spectrometry (SIMS, Fig. 10.6). In SIMS, a beam of primary ions is focused onto a solid sample in the presence of a strong electric field. The primary beam sputters atoms from the surface, some of which get ionised and transferred into a mass spectrometer. Either a Cs^+ beam is used to generate negative secondary ions of electronegative elements (e.g., C, O, S, etc.) or an O^- beam is used to generate positive ions of electropositive species (e.g., Mg, Ti etc.). SIMS combines high sensitivity with high spatial resolution to allow isotopic ratios of even minor elements to measured in very small samples and was crucial in the discovery and detailed isotopic characterisation of pre-solar grains. Modern SIMS instruments, e.g., the Cameca NanoSIMS (Fig. 10.6) and ims-1280 ion probes, include very high transmission of secondary ions and multi-collection detector systems. In the case of the NanoSIMS, a resolution of <100 nm can be attained with a Cs^+ source, compared to the best resolution of ~1 μm with previous instruments. These characteristics allow higher-precision data to be acquired on smaller spatial scales than was ever possible before, allowing, for example, detailed isotopic characterisation of sub-micron pre-solar grains (Nguyen and Zinner 2004; Zinner et al. 2005) as well as high-precision ^{26}Al systematics on small scales in meteoritic inclusions (Kita et al. 2012) and in cometary samples returned by NASA's Stardust mission (Matzel et al. 2010).

An extraordinarily useful feature of SIMS instruments is the ability to produce mass-filtered images of a sample. Two types of SIMS imaging are commonly used in meteoritic research. In *direct imaging,* the instrument behaves as a microscope: the primary beam is defocused on the sample and the ion optics of the instrument transfer an image of the surface through the mass spectrometer onto an imaging detector (e.g., a micro-channel plate or a CCD). The spatial resolution of this technique is set by the ion optics and is typically >500 nm. In *scanning* or *raster* imaging, a focused beam is scanned over the sample with synchronised collection of secondary ions; spatial resolution is set by the size of the primary beam (>50 nm in the NanoSIMS). Both techniques are extremely useful for scanning large numbers of meteoritic grains to search for isotopically anomalous, pre-solar grains of stardust (Nguyen and Zinner 2004; Nittler et al. 1994; Nagashima et al. 2004). Examples of NanoSIMS raster imaging are shown in Fig. 10.8. In the top panels, O isotopic ratio images of an area of a primitive meteorite clearly reveal two sub-micrometer

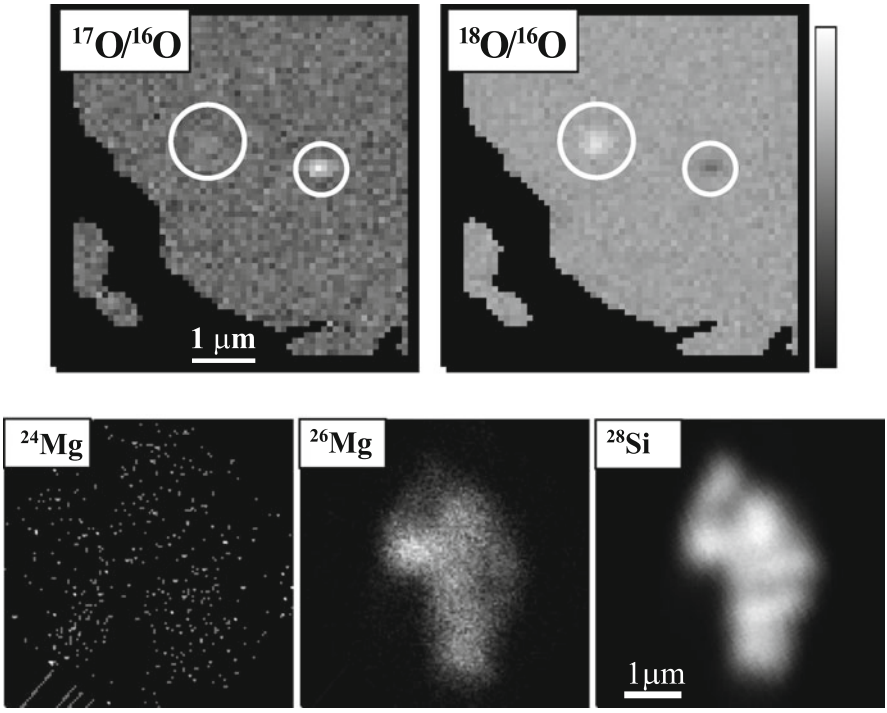

Fig. 10.8 Example NanoSIMS isotopic images of presolar grains. Top Panels: Isotopic images of a $5 \times 5\,\mu m^2$ area of a primitive meteorite; circles indicate highly anomalous presolar grains surrounded by isotopically normal (solar-composition) material (Nguyen et al. 2010). Bottom panels: Isotopic images of a pre-solar SiC grain from a supernova. Mg in this grain is mono-isotopic ^{26}Mg, due to decay of ^{26}Al (Nittler et al. 2007)

grains with anomalous ^{17}O and ^{18}O abundances (circled). In the bottom panels, a SiC grain believed to have originated from a supernova is revealed to have mono-isotopic ^{26}Mg, from *in situ* decay of ^{26}Al (the inferred ^{26}Al/^{27}Al ratio for this grain is $\sim$0.5).

Additional *in situ* techniques used in meteoritic radioactivity research include laser-heating noble-gas analyses and Resonance Ionisation Mass Spectrometry (RIMS). In the former, a sample is melted with a laser, releasing atoms of noble gases trapped within. These gases are collected, ionised by bombarding them with electrons and measured with a mass spectrometer. This technique has been successfully applied to He and Ne isotopes in individual pre-solar grains of graphite and SiC, in some cases providing evidence of extinct ^{22}Na (Heck et al. 2007). RIMS uses lasers to ablate material from samples and then to selectively ionise atoms of a specific element; these are measured by means of a time-of-flight mass spectrometer. This technique has extraordinary sensitivity for the selected element and eliminates isobaric interferences that precludes measurement of some isotopes by SIMS. It has

provided extremely useful isotopic data for trace elements within single pre-solar grains, including Zr, Mo, Ba, and Ru (Nicolussi et al. 1997; Savina et al. 2004).

A fundamental question for analysis of small samples like pre-solar grains is whether a given isotopic signature might be detectable in a given sample. Because *in situ* isotopic measurements are governed by Poisson statistics, the answer depends on the total number of atoms of the isotope of interest that can be detected, which clearly depends on the specific problem. The number of detectable atoms depends on the abundance of the element in the sample (determined by chemistry), the size of the sample (giving the total number of atoms) and the efficiency of the instrument (giving the fraction of atoms in a sample that can actually be detected and counted). For SIMS, the latter efficiency typically ranges from 10^{-7} to 10^{-2} and depends both on the low ionisation probability of secondary ions during the sputtering process and the efficiency of transmitting ions through the mass spectrometer. As an example, let us consider the detection by SIMS of extinct ^{26}Al in pre-solar SiC grains. A 1-µm SiC grain contains some 5×10^{10} atoms. Assuming an initial ^{26}Al/^{27}Al ratio of 10^{-3}, a typical Al concentration of 1% in pre-solar SiC, and a detection efficiency of 10^{-2}, consuming an entire 1-µm grain would yield some 5000 atoms of radiogenic ^{26}Mg, corresponding to a statistical uncertainty of ~1.4%. Measuring only a fraction of the grain (to preserve it for additional isotopic analyses, for instance), or smaller grains, or grains with lower initial ^{26}Al contents would correspondingly lower the number of detected atoms and decrease the precision. Moreover, whether the radiogenic signature is observable depends also on the amount of non-radiogenic Mg present in the grain. Clearly, similar considerations must be made for any given problem at hand.

10.2.4 Perspectives for Astronomy with Meteorite Samples

As in many fields, the technology for chemical and isotopic analysis of geological and cosmo-chemical materials is rapidly evolving and improving and this will certainly continue into the future. Recent improvements in the stability of commercial instruments and advances in chemical treatments used to purify samples are now providing for extremely high precision measurements of bulk samples by TIMS and ICP-MS (Brennecka et al. 2010; Budde et al. 2016) and of intermediate-scale (tens of microns) *in situ* analyses by SIMS (Villeneuve et al. 2009). For analysis of tiny samples like pre-solar grains, significant effort is being expended to improve both sensitivity and spatial resolution. While the NanoSIMS has long achieved sub-100 nm spatial resolution with a Cs^+ primary ion source, the duoplasmatron commonly used to generate O^- beams can achieve at best ~400–500 nm. However, a new RF plasma-based O^- ion source, developed by Oregon Physics, LLC, can match the spatial resolution of the Cs^+ beam and has been installed on several ion microprobes (Matzel et al. 2014; Liu et al. 2018). This source will greatly improve measurements of key radionuclides like ^{26}Al, ^{41}Ca, and ^{60}Fe in ever-smaller meteoritic samples and pre-solar grains.

While SIMS has the advantage of achieving high spatial resolution, it is fundamentally limited by the low ionisation probability for secondary ions during sputtering. In contrast, previous RIMS instruments have proven to have extraordinary sensitivity for certain elements, but limited spatial resolution due to the use of lasers to ablate atoms from samples. A new instrument, named CHILI (CHicago Instrument for Laser Ionisation), has been developed in recent years at the University of Chicago (Stephan et al. 2016) and combines a very high resolution sputtering Ga^+ ion gun with multiple lasers for resonance ionisation to achieve both sensitivity and spatial resolution beyond what is currently possible. As of this writing, the instrument is generating important data on pre-solar grains and other meteoritical problems with a laser ablation source (Liu et al. 2017; Trappitsch et al. 2018; Stephan et al. 2018; Kodolányi et al. 2018) while development of the scanning Ga sputtering source is ongoing.

Another approach is to use the front end of a commercial SIMS instrument to produce secondary ions which are then further accelerated to 300–1000 keV energies allowing for highly efficient suppression of molecular interferences, and thus allowing for higher sensitivity. The first such instrument, the *MegaSIMS* constructed at the University of California, Los Angeles (McKeegan et al. 2009), was developed specifically for analysis of solar-wind samples returned by NASA's Genesis mission. More recently, a similar instrument called SIMS-SSAMS has been developed at the United States Naval Research Laboratory (Groopman et al. 2017). With its micron-scale spatial resolution and high sensitivity, this instrument has great promise for addressing many problems in meteoritical science.

A fundamentally different technology, atom probe tomography, also holds great promise for isotopic and analysis of small extraterrestrial samples. In an atom probe, the sample is embedded in a very small, extremely sharp tip with a high potential applied to it. Applying a laser to the tip allows for single atoms to be extracted from the tip, one by one, and transmitted to a mass spectrometer. Reconstruction of atom trajectories allows the 3-dimensional reconstruction of the original positions and chemical identity of up to tens of millions of individual atoms. Technical limitations have thus far mostly limited the use of atom probe tomography to materials science applications, but recent attempts to apply the technique to pre-solar grains (Heck et al. 2014) suggest that it is likely to become a very useful tool for cosmochemistry in coming years.

10.3 Detection and Analysis of Cosmic Rays

The discovery of Galactic cosmic rays was inextricably tied to the development of sub-atomic particle physics in the early decades of the twentieth century. In particular, the discoveries in 1912–1914 by Hess and Kolhörster, through high-altitude balloon flights, of a source of ionisation that increases with altitude clearly indicated an extraterrestrial source of high-energy radiation (see historical review in Longair 1992). Through the decades, increasingly more sophisticated instruments

and experiments have been developed and deployed to determine the composition and energy spectra of cosmic rays. Because primary cosmic rays cannot penetrate the Earth's thick atmosphere to be detected at the ground, balloon-borne and space-based experiments remain crucial to progress in cosmic ray physics to the present day. However, due their very low flux, ground-based telescopes are still required to detect the highest-energy cosmic rays, through the *air showers* of secondary particles they produce as they traverse the atmosphere. This section describes some of the basic techniques used to detect and characterise GCRs both from the ground and at high altitudes.

10.3.1 Ground-Based Observations

When Galactic cosmic rays enter the Earth's atmosphere, they interact with its atoms and molecules, generating a cascade of secondary particles. For most cosmic rays, these cascades overlap and lead to a relatively constant flux at ground level of secondary particles, dominated by muons. In contrast, air showers are caused by single primary cosmic rays with sufficient energy that their secondary particle cascades are detectable at ground level. Modern ground-based cosmic-ray telescopes are comprised of vast areas of particle and light detectors, designed to detect and characterise as many secondary particles as possible and hence reconstruct the characteristics of the original high-energy cosmic ray. For example, the largest such facility in the world, the Pierre Auger Observatory, is planned to ultimately include sites in Argentina and Colorado; the southern site is operational. It uses two common types of air shower detectors: an array of 1600 water tank detectors spaced out over some 3000 km^2 surrounded by four inward-looking *fluorescence detectors* (FDs) (The Pierre Auger Collaboration et al. 2007). The water tanks detect high-energy particles through the Cherenkov light they emit while passing through the tanks (essentially an electromagnetic sonic boom since the speed of light in the water is smaller than the particle velocities). The FDs consist of telescopes designed to detect UV fluorescent light from interaction of the shower particles with atmospheric nitrogen. Together, the two types of detectors allow reconstruction of the initial energy and direction of the primary cosmic ray. Similar techniques are used in other large air shower experiments, such as HiRes (Abbasi et al. 2004, 2008) and AGASA (Takeda et al. 2003).

10.3.2 High-Altitude and Space-Based Observations

As a charged particle passes through matter, it loses energy through ionisation of atoms and molecules of the material. These ionisation losses can cause significant damage to crystal structures and molecular chains. Many early studies of the composition of cosmic rays took advantage of this radiation damage in certain

materials, such as many plastics as well as minerals in meteorites and lunar samples. The damaged areas have much higher chemical reactivity than the undamaged material. Thus, chemical etching of the materials reveals *tracks*, the nature (e.g., size) of which can be empirically related to the identities and energies of the incident particles (Fleisher et al. 1975). This technique was used starting in the late 1960s with balloon-borne plastic detectors to identify elements heavier than Fe, including heavy radioactive elements like U, in the primary GCRs (Blanford et al. 1969).

Because of limitations in the track technique (e.g., relatively poor resolution in charge identification), modern determinations of the composition of Galactic cosmic rays are based on electronic measurements of the total energy and energy loss rate as incident particles pass through various combinations of detectors. The rate of energy loss, $-dE/dx$, is proportional to the square of the particle's charge and depends also on its velocity as well as properties of the material (the Bethe-Bloch formula, Longair 1992). If both $-dE/dx$ and the total kinetic energy can be independently determined, the charge and mass of the particle can be inferred. In practice, stacks of detectors are used to determine these parameters and additional detectors can be used to refine particle trajectories and exclude backgrounds. Examples of modern cosmic-ray experiments are given below.

Detectors used for cosmic-ray experiments commonly include: *solid-state detectors*, Si or Ge crystals in which the incident radiation releases electron-hole pairs that can be measured as an electrical pulse; *scintillation detectors*, crystals (e.g., NaI or certain plastics) in which light is produced by the incident radiation and detected by photomultiplier tubes; *Cherenkov detectors,* a type of scintillator for which particles above a threshold energy emit detectable light; and *transition radiation detectors,* stratified detectors with different indices of refraction; X-rays are emitted when particles cross the interfaces, with the amount of radiation dependent on the velocity of the particle.

A wealth of data on the isotopic and elemental composition of GCR nuclei has been obtained in the last two decades by the Cosmic Ray Isotope Spectrometer (CRIS, Stone et al. 1998) on the *Advanced Composition Explorer* satellite, launched by NASA in 1997 and still operational as of this writing (Binns et al. 2016). A schematic diagram of the CRIS instrument is shown in Fig. 10.9 (from George et al. 2009). The instrument consists of a position sensitive *hodoscope* detector (HNX,Y) to determine particle trajectories and stacks of solid-state Si detectors (E1–E9) to measure energy and energy loss rate. The hodoscope is constructed of layers of criss-crossed scintillating plastic fibers coupled to image-intensified CCD detectors. As a particle passes through the layers, the patterns of light observed on the CCDs can be inverted to determine the trajectory of the particle through the instrument with high precision. Additional layers of scintillating fibers at the top (TX,TY) serve as a trigger to signal the instrument that a particle has arrived. The arrow indicates the trajectory of a particle that enters the instrument and is finally stopped in the Si layer E9. For this event, the signals measured in detectors E1–E6 provide a measure of the energy loss rate ($-dE/dx$) whereas the total energy is found from that deposited in all seven detectors.

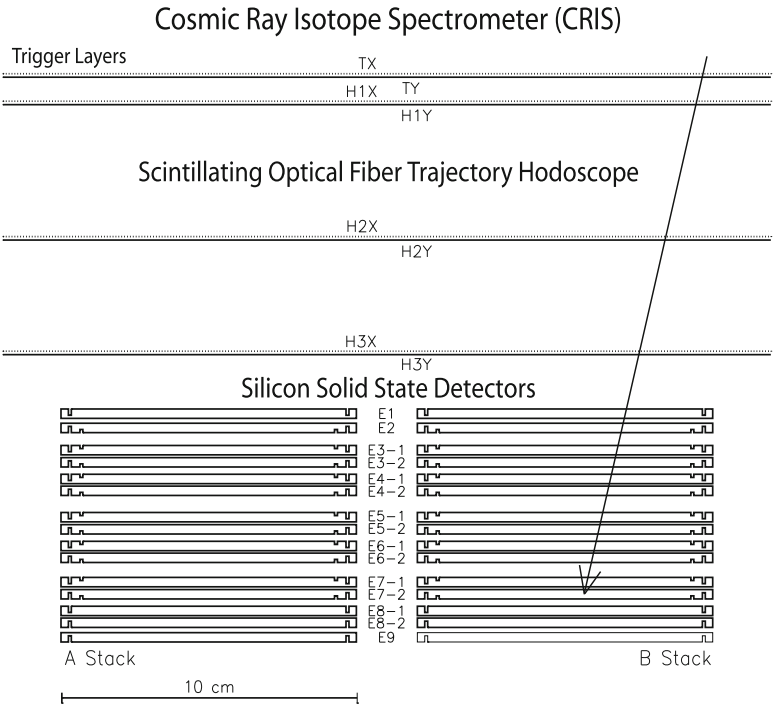

Fig. 10.9 Schematic of CRIS instrument on the *Advanced Composition Explorer* satellite, from George et al. (2009). Arrow indicates the trajectory of a single particle entering the instrument

The process of particle discrimination in CRIS is illustrated in Fig. 10.10 (Stone et al. 1998), showing data obtained with a CRIS Si detector stack from a laboratory calibration experiment. Each data point represents the energy lost in detectors E1 through E3 plotted against the energy deposited in E4 for a single particle traversing the detector stack. Curves corresponding to the distinct isotopes of the indicated elements are clearly seen.

Other modern GCR composition instruments and experiments are designed around similar principles though with widely varying details. For example, the Trans-Iron Galactic Element Recorder (TIGER) experiment, flown on high-altitude balloons in Antarctica in 2001 and 2003, used a combination of scintillation and Cherenkov detectors to determine the composition of GCR with atomic number $26 < Z < 38$ (Rauch et al. 2009). To determine the composition of GCR at higher energies than studied by the experiments described above, the Transition Radiation Array for Cosmic Energetic Radiation (TRACER) instrument uses a combination of Cherenkov, scintillator, gas-filled proportional counter and transition radiation detectors (Ave et al. 2008).

The instruments described above are designed to detect and characterise the composition of GCR nuclei. As discussed in Chap. 7, cosmic-ray positrons also

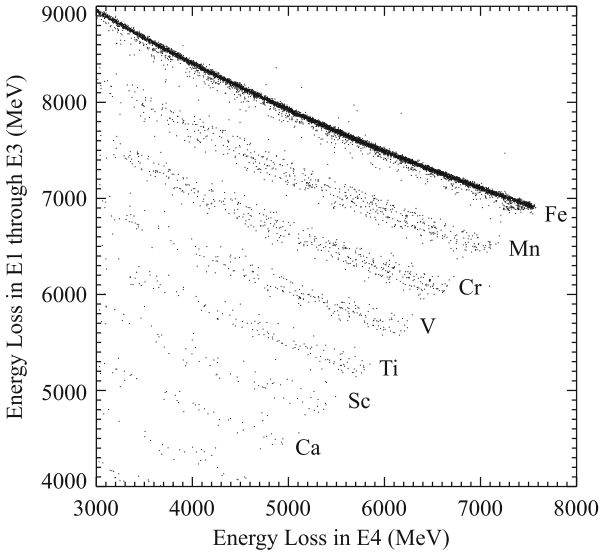

Fig. 10.10 Calibration data for CRIS: plot of energy deposited in Si detectors E1–E3 versus that in detector E4. Particles of a given mass and charge plot along distinct curves, allowing isotope discrimination. Figure taken from Stone et al. (1998)

provide important information regarding the origin and interactions of GCRs in the Galaxy. In 2009 it was reported that the positron fraction of cosmic rays increases with increasing energy, inconsistent with purely secondary sources, based on data from the PAMELA instrument on board the Russian Resurs-DK1 satellite, launched in 2006 (Adriani et al. 2009). PAMELA is broadly similar to other instruments designed to identify positrons (e.g., HEAT, Barwick et al. 1997) and consists of scintillator detectors to measure time of flight and dE/dx for traversing particles and to distinguish upward-traveling electrons from downward-traveling positrons, a magnetic spectrometer to measure the rigidity (momentum per unit charge) of the particles, and an electromagnetic calorimeter consisting of interleaved layers of W absorbers and solid-state Si detectors. The calorimeter allows positrons to be distinguished from protons and anti-protons from electrons in the instrument. More recently, this positron excess has been confirmed and clarified with the Alpha Magnetic Spectrometer that operated on the International Space Station in 2011–2013 (Aguilar et al. 2013; Accardo et al. 2014).

References

Abbasi RU, Abu-Zayyad T, Amann JF et al (2004) Phys Rev Lett 92:151101
Abbasi RU, Abu-Zayyad T, Allen M et al (2008) Phys Rev Lett 100:101101
Accardo L, Aguilar M, Aisa D et al (2014) Phys Rev Lett 113:121101

Adriani O, Barbarino GC, Bazilevskaya GA et al (2009) Nature 458:607
Aguilar M, Alberti G, Alpat B et al (2013) Phys Rev Lett 110:141102
Atwood WB, Abdo AA, Ackermann M et al (2009) Astrophys J 697:1071
Ave M, Boyle PJ, Gahbauer F et al (2008) Astrophys J 678:262
Barwick SW, Beatty JJ, Bhattacharyya A et al (1997) Astrophys J 482:L191
Binns WR, Israel MH, Christian, ER et al (2016) Science 352:677
Blanford GE, Friedlander MW, Klarmann J et al (1969) Phys Rev Lett 23:338
Boggs S, Kurfess J, Ryan J et al (2006) Presented at the Society of Photo-Optical Instrumentation Engineers (SPIE) conference. Society of Photo-Optical Instrumentation Engineers (SPIE) conference series, vol 6266
Brennecka GA, Weyer S, Wadhwa M et al (2010) Science 327:449
Budde G, Burkhardt C, Brennecka GA et al (2016) Earth Planet Sci Lett 454:293
De Angelis A, Tatischeff V, Tavani M et al (2017) Exp Astron 44:25
Diehl R, Siegert T, Greiner J et al (2017) ArXiv e-prints, 1710.10139
Fleisher RL, Price PB, Walker RM (1975) Nuclear tracks in solids: principles and applications. University of California Press, Berkeley
Forrest DJ, Chupp EL, Ryan JM et al (1980) Sol Phys 65:15
George JS, Lave KA, Wiedenbeck ME et al (2009) Astrophys J 698:1666
Gray CM (1974) Nature 251:495
Greiner J, Iyudin A, Kanbach G et al (2009) Exp Astron 23:91
Groopman EE, Grabowski KS, Fahey AJ, Koop L (2017) J Anal At Spectrom 32:2153
Harrison FA, Craig WW, Christensen FE et al (2013) Astrophys J 770:103
Heck PR, Marhas KK, Hoppe P et al (2007) Astrophys J 656:1208
Heck PR, Stadermann FJ, Isheim D et al (2014) Meteorit Planet Sci 49:453
Kanbach G, Bertsch DL, Favale A et al (1989) Space Sci Rev 49:69
Kanbach G, Andritschke R, Bloser PF et al (2003). In: Truemper JE, Tananbaum HD (eds) Presented at the Society of Photo-Optical Instrumentation Engineers (SPIE) conference. Society of Photo-Optical Instrumentation Engineers (SPIE) conference series, vol 4851, pp 1209–1220
Kierans CA, Boggs SE, Chiu J-L et al (2017) ArXiv e-prints, 1701.05558
Kita NT, Ushikubo T, Knight KB et al (2012) Geochim Cosmochim Acta 86:37
Knie K, Korschinek G, Faestermann T et al (2004) Phys Rev Lett 93:171103
Knödlseder J (2007) Adv Space Res 40:1263
Kodolányi J, Stephan T, Trappitsch R et al (2018) Geochim Cosmochim Acta 221:127
Lee D, Halliday AN (1995) Nature 378:771
Lee T, Papanastassiou DA, Wasserburg GJ (1976) Geo Res Lett 3:41
Liu N, Stephan T, Boehnke P et al (2017) Astrophys J 844:L12
Liu M-C, McKeegan KD, Harrison TM, Jarzebinski G, Vltava L (2018) Int J Mass Spectrom 424:1
Longair MS (1992) High energy astrophysics (1992) Vol. 1: Particles, photons and their detection (High energy astrophysics, by MS Longair. Cambridge University Press, Cambridge, pp. 436. ISBN 0521387736
Matzel JEP, Ishii HA, Joswiak D et al (2010) Science 328:483
Matzel JEP, Ishii HA, Joswiak D, Brownlee D, Hutcheon ID (2014) Lunar and Planetary Institute Technical Report. Lunar and planetary science conference, vol 45, p 1645
McEnery JE (2017) AAS/High energy astrophysics division, vol. 16. AAS/High Energy Astrophysics Division, 103.13
McKeegan KD, Kallio AP, Heber V et al (2009) Lunar and Planetary Institute Science conference abstracts. Lunar and Planetary Institute Science conference abstracts, vol 40, p 2494
Nagashima K, Krot AN, Yurimoto H (2004) Nature 428:921
NCT Collaboration, Boggs S, Chang Y (2007) Adv Space Res 40:1281
Nguyen AN, Zinner E (2004) Science 303:1496
Nguyen AN, Nittler LR, Stadermann FJ, Stroud RM, Alexander CMO (2010) Astrophys J 719:166
Nicolussi GK, Davis AM, Pellin MJ et al (1997) Science 277:1281
Nittler LR, Alexander CMO'D, Gao X, Walker RM, Zinner EK (1994) Nature 370:443

Nittler LR, Hoppe P, Stroud RM (2007) Lunar and planetary science conference 38, Abstract #2321
Rauch BF, Link JT, Lodders K et al (2009) Astrophys J 697:2083
Savina MR, Davis AM, Tripa CE et al (2004) Science 303:649
Schönfelder V, Aarts H, Bennett K et al (1993) Astrophys J Suppl 86:657
Stephan T, Trappitsch R, Davis AM et al (2016) Int J Mass Spectrom 407:1
Stephan T, Trappitsch R, Davis AM et al (2018) Geochim Cosmochim Acta 221:109
Stone EC, Cohen CMS, Cook WR et al (1998) Space Sci Rev 86:285
Takahashi T, Awaki A, Dotani T et al (2004). In: Hasinger G, Turner MJL (eds) Proceedings of SPIE. UV and gamma-ray space telescope systems, vol 5488, pp 549–560
Takahashi T, Kelley R, Mitsuda K et al (2009). In: Kawai N, Mihara T, Kohama M, Suzuki M (eds) Astrophysics with all-sky X-ray observations, p 356
Takeda M, Sakaki N, Honda K et al (2003) Astropart Phys 19:447
The Pierre Auger Collaboration, Abraham J, Abreu P et al (2007) Science 318:938
Trappitsch R, Stephan T, Savina MR et al (2018) Geochim Cosmochim Acta 221:87
Vedrenne G, Roques J, Schönfelder V et al (2003) Astron Astrophys 411:L63
Vestrand WT, Share GH, Murphy RJ et al (1999) Astrophys J Suppl 120:409
Villeneuve J, Chaussidon M, Libourel G (2009) Science 325:985
Weidenspointner G, Harris MJ, Sturner S, Teegarden BJ, Ferguson C (2005) Astrophys J Suppl 156:69
Young ED, Simon JI, Galy A et al (2005) Science 308:223
Zinner E, Nittler LR, Hoppe P et al (2005) Geochim Cosmochim Acta 69:4149
Zych AD, O'Neill TJ, Bhattacharya D et al (2006) Presented at the Society of Photo-Optical Instrumentation Engineers (SPIE) conference. Society of Photo-Optical Instrumentation Engineers (SPIE) conference series, vol 6319